Available online at www.sciencedirect.com
SCIENCE DIRECT
Journal of the European Ceramic Society 26 (2006) 1325–1335
www.elsevier.com/locate/jeurceramsoc

Hard silicon carbonitride films obtained by RF-plasma-enhanced chemical vapour deposition using the single-source precursor bis(trimethylsilyl)carbodiimide

Yanping Zhou [a,b,*], Daniel Probst [c], Andreas Thissen [a], Edwin Kroke [b], Ralf Riedel [a], Ralf Hauser [a], Holger Hoche [c], Erhard Broszeit [c], Peter Kroll [d], Herbert Stafast [e]

[a] *Darmstadt University of Technology, Institute of Materials Science, Petersenstrasse 23, 64287 Darmstadt, Germany*
[b] *Department of Chemistry, University of Konstanz, Fach M 736, 78457 Konstanz, Germany*
[c] *State Materials Testing Institute Hessen, Chair and Institute for Materials Technology, Darmstadt University of Technology, Grafenstraße 2, 64283 Darmstadt, Germany*
[d] *Institute of Inorganic Chemistry, Aachen University of Technology, Prof.-Pirlet-Str. 1, 52074 Aachen, Germany*
[e] *IPHT Jena e.V., POB 100239, D-07702 Jena, Germany*

Received 21 October 2004; received in revised form 2 February 2005; accepted 4 February 2005
Available online 19 March 2005

Abstract

Amorphous silicon carbon nitride (Si/C/N) coatings were prepared on steel substrates by RF plasma-enhanced chemical vapour deposition (RF-PECVD) from the single-source precursor bis(trimethylsilyl)carbodiimide (BTSC). The films were characterised by X-ray diffraction (XRD), ellipsometry, FTIR, glow discharge optical emission spectroscopy (GDOES), optical microscopy, AFM, hardness measurements, scratch-, tribological- and corrosion-tests. The results of these studies show that the coatings obtained on the RF-powered electrode (cathode) were black, thick (>20 μm) and hard (21–29 GPa), while those grown on the grounded electrode (anode) were yellow, thin (<4 μm) and soft (∼5 GPa). Coatings on the anode contained around 19 at.% oxygen and exhibited silicon predominantly bonded to oxygen. In contrast, the oxygen content of the films deposited on the cathode was below 2 at.%. Silicon atoms in these coatings are co-ordinated predominantly to nitrogen and carbon. The surface of all coatings was very smooth with a maximum rms roughness between 2 nm and 5 nm for an area of 5 μm × 5 μm. Scratch and tribological tests reveal a brittle nature of the cathode-coatings and rather weak adhesion to the metal substrates. Salt-spray tests indicate an excellent corrosion resistance of the material.

Keywords: Si/C/N; Films; Hardness; Wear resistance; PECVD

1. Introduction

Amorphous and crystalline silicon carbonitride materials have received much attention in recent years due to their attractive properties such as outstanding oxidation resistance at elevated temperatures and high hardness.[1] Silicon carbonitride films have potential for applications in wear or corrosion protection[2] as well as microelectronic and optoelectronic devices.[3]

There have been many studies on the fabrication of silicon carbonitride film by various techniques, including both physical vapour deposition (PVD)[4–7] and chemical vapour deposition (CVD).[3,8–18] Among the CVD methods, plasma-enhanced (PE) or plasma-assisted (PA) CVD is most promising for the low-temperature deposition of Si/C/N films.[3,11,15–17] Most metals have relatively low melting points, therefore, in the case of metallic materials used as substrates, coatings must be prepared at significantly lower temperatures than the melting point of the metal in order to avoid thermal damage. Many researchers have reported on PECVD of Si/C/N using silane (SiH_4) as the silicon source.[3,15–18]

* Corresponding author. Tel.: +49 6151 166341; fax: +49 6151 166346.
E-mail address: zhou@materials.tu-darmstadt.de (Y. Zhou).

0955-2219/$ – see front matter © 2005 Elsevier Ltd. All rights reserved.
doi:10.1016/j.jeurceramsoc.2005.02.004

The single-source precursor most frequently used for Si/C/N-coatings is hexamethyldisilazane (HMDS).[8–13] Furthermore, bulk Si/C/N ceramics and glasses were prepared using polymer pyrolysis as well as related routes.[19,20] Interestingly, the properties of the products strongly depend not only on the composition but also on the structure of the organometallic precursor. This strongly suggests that the structure and properties of silicon carbonitride ceramics can be modified and controlled by selecting and designing suitable precursors and processing parameters.[21] Similar conclusions can be drawn from the results of single-source precursor based vapour phase deposition approaches to generate Si/C/N coatings.[22]

In previous studies we synthesised several Si/C/N polymers starting from bis(trimethylsilyl)carbodiimide (BTSC) and chlorosilanes. The solid and liquid precursors were pyrolytically transformed into bulk silicon carbide, silicon nitride and ternary Si/C/N phases.[23] In this work, the aim was to study of hard thin film formation on the steel surface from BTSC precursor by PECVD method. We will report the preparation of hard Si/C/N films on high-speed cutting steel S652 metal substrates using BTSC as a single-source liquid precursor for PECVD for the first time.

2. Experimental part

The Si/C/N films were deposited in a vertical parallel plate capacitance coupled RF-PECVD system. The RF-PECVD apparatus consists of five major parts: a discharge reactor, a RF power system, a pumping system, a heater, and a gas supply system. The stainless steel reactor main tube is 150 mm in length and 153 mm in inner diameter. A radio frequency generator (13.56 MHz, Dressler, model CESAR 136) supplied RF power to the reactant gas mixture through an impedance matching box network (Dressler, VM600A). The evacuation system consisted of a turbomolecular pump (Edwards EXT70/NW50 with a RV3 rotary vane pump and EXC120 controller) and a two-stage rotary oil pump (Edwards E2M18).

The single-source precursor bis(trimethylsilyl)carbodiimide $(CH_3)_3Si\text{-}NCN\text{-}Si(CH_3)_3$ was synthesised as described in the literature.[24] Preliminary experiments indicated that the vapour pressure of BTSC at room temperature is too high. Therefore, the precursor was kept at 0 °C with an ice bath and evaporated by an argon carrier gas stream, which was bubbled through the liquid. Prior to deposition, the reactor was evacuated to $<10^{-5}$ mbar for cleaning. The partial pressures of BTSC and argon inside the discharge reactor were controlled by plug valves and mass flow controllers (Bronkhorst F-201C-FAC-33-V and F-200C-FA-88-V).

The total pressure (P_{tot}) was set to 0.3 mbar and the temperature (T_{dep}) of the grounded electrode GE (anode) was kept at 300 °C. The RF electrode (cathode) was not heated, its temperature depends on the RF power and the deposition conditions. The distance between the two electrodes was 18 mm. The films were deposited on polished high speed cutting steel S652 substrates placed on both the RF electrode and the grounded electrode. RF-induced negative DC self-bias, V_B, developed on the RF electrode. Prior to deposition, the substrates were cleaned ultrasonically in acetone and in an argon plasma in order to remove any contaminants and to activate the metal surface to achieve good film adhesion.

The film thickness was determined by ellipsometry (Sentech SE 850) and the ball cratering method (with a self-designed device) in the case of the thicker and non-transparent coatings, respectively. The films were investigated by X-ray diffraction (XRD, Seifert, PTS 3000) using Cu Kα radiation. The chemical structure of the deposited films were analysed by FTIR (Perkin-Elmer 1750) with an ATR-unit. All as-received coatings on the steel surface were directly inspected by XRD and FTIR. The depth profiles of the Si, C, N, O and H content of the films were obtained using glow discharge optical emission spectroscopy (GDOES, Spektruma GDA 750). Surface morphology and topography were observed by optical microscopy and AFM (Thermomicroscopes CP) with a 100 μm scanner. The root-mean-squared (rms) roughness of the films was also estimated after the polynomial background correction in the third order line by line. The rms roughness is given by the standard deviation of the data, determined using the standard definition: $R_{rms} = \sqrt{\sum_{n=1}^{N}(Z_n - \bar{Z})^2/(N-1)}$, where $\bar{z}$ = mean z height. The rms roughness refers only to the included areas defined by a region group. The measurement is referenced to the mean height of the data within the area defined by that region group. The hardness of the as-received coatings was determined with the instrumented indentation testing method in reference to DIN EN ISO 14577-1 using a Shimadzu DUH 202 ultra microhardness tester equipped with a Vickers shaped diamond at testing loads of 10 mN and 100 mN. Additionally the elastic moduli were calculated from the indentation curves. Because the coating adhesion is of crucial importance for tribological applications, the adhesion and cohesion of the films were investigated by using a CSEM Revetest scratch tester according to DIN 1071-3. The coating is drawn under a Rockwell C diamond at a constant feed of 10 mm/min and acoustic emission and tangential forces were recorded online while increasing the load at a rate of 10 N/mm. Concerning the adhesion and cohesion failure morphologies the scratches were investigated using an optical microscope.

The samples coated on the cathode side were investigated with respect to their wear properties during oscillating friction. A SRV III optimol high-temperature tribometer was used for the investigation in the ball on disk geometry. The instrument calculates the complete wear of the system by measuring the overall change of the vertical position of the ball-holding unit during the test. Friction and wear coefficients are also recorded online, allowing for abortion of the test immediately when a drastic change in either parameter occurred. Thereby examination and determination of causes for the film failure is possible. In the test cycle a pin-type counterbody (100Cr6 ball, Ø 10 mm) oscillates while

exerting a defined force onto the film. A standard roller bearing steel ball was used. The test was conducted in lubricated condition as well as dry at varying test temperatures: The tests were carried out with lubrication, under a load of 5 N normal force, at RT and 100 °C and at 30 N as well as 50 N normal force, at RT. Without lubrication a normal force of 5 N was used and the testing temperature was RT and 400 °C. The test was stopped automatically after 60 min (180,000 cycles or 432 m) or after coating failure. The wear tracks were examined using a Zeiss DSM962 scanning electron microscope (SEM) with Noran Vantage EDX system to determine the wear mechanisms and to identify the wear products. The geometry of the wear tracks was analysed by profilometry using a Hommel tester T8000.

For corrosion testing, samples were submitted to a 96 h salt-spray test according to DIN 50021. The free corrosion potential was determined in 3% NaCl solution. Current density-potential curves were recorded in 0.1% NaCl solution using the samples as test electrodes, a silver–silver chloride electrode and a potentiostat.

3. Results

In Table 1 we list PECVD conditions of the deposition process and properties of received coatings for four representative experiments. While we will focus on the properties in more detail, we observe a very general trend: chemical composition and mechanical properties of coatings received at the RF electrode are very different from those deposited on the grounded electrode.

3.1. Chemical and microstructural characterisation

The XRD patterns of all films show only such reflections which can be assigned to the substrate (S652 steel), i.e., primarily α-Fe. No traces of crystalline SiC, Si_3N_4, Si_2N_2O, SiO_2 or other phases were found, which indicated the amorphous nature of the coatings. Analysing the chemical composition of the coatings with GDOES measurements revealed a homogenous distribution of the elements throughout the film, except for a small oxidised surface layer. Corresponding depth profiles of the films SBIS21-rf and SBIS21 are presented in Fig. 1. They indicate a substantial oxygen content of the coating deposited at the grounded electrode (SBIS21). Even at a depth of 1 μm the oxygen content is about 17 at.%, and thus larger than the nitrogen content. Furthermore, oxygen accumulates at the interface between coating and substrate. The Si:N ratio of these highly oxidised films is about 1:1, the Si:C ratio approximately 1:3. Coatings received at the RF electrode (SBIS21-rf), however, are almost oxygen free, even though deposited in the same experiment. Moreover,

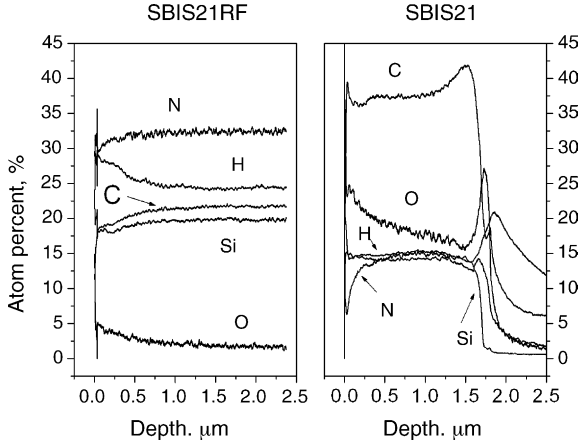

Fig. 1. Typical GDOES profiles of the chemical composition of the Si/C/N films: SBIS21-rf (RF electrode) and SBIS21 (grounded electrode) specimens. The measurements reveal constant compositions in the bulk of the films. The Si, C, N, O and H concentrations in Table 1 represent these constant values.

Table 1
PECVD conditions and film characteristics

Sample	Growth site[a]	RF power (W)	Bias (V)	Substrate temperature (°C)	Deposition time (min)	Thickness (μm)	GDOES composition	Elastic modulus (100 mN) (GPa)	Plastic hardness (100 mN) (GPa)
SBIS24-rf	RF	12∼25[b]	−500	n.d.[c]	60	>20	$SiN_{1.89}C_{1.10}O_{0.04}H_{1.00}$	93.8	29.0 ± 7.3
SBIS24	GE	12∼25[b]	0	300	60	1.86	$SiN_{1.13}C_{2.69}O_{1.09}H_{1.14}$	84.3[d]	4.5 ± 0.3
SBIS21-rf	RF	12∼30[b]	−500	n.d.[c]	60	>20	$SiN_{1.64}C_{1.09}O_{0.10}H_{1.24}$	88.5	26.5 ± 1.4
SBIS21	GE	12∼30[b]	0	300	60	1.34	$SiN_{1.00}C_{2.62}O_{1.35}H_{1.05}$	83.1[d]	4.8 ± 0.3
SBIS20-rf	RF	11∼−35[b]	−500	n.d.[c]	90	>20	n.d.[c]	81.3	21.2 ± 4.6
SBIS20	GE	11∼35[b]	0	300	90	2.95	$SiN_{1.08}C_{2.62}O_{1.25}H_{1.09}$	63.7[d]	4.3 ± 0.1
SBIS19-rf	RF	30	−358∼−406[e]	n.d.[c]	90	>20	$SiN_{1.66}C_{1.10}O_{0.08}H_{1.15}$	109.2	28.6+/−7.9
SBIS19	GE	30	0	300	90	3.02	$SiN_{1.17}C_{4.45}O_{1.24}H_{1.19}$	61.0[d]	4.5 ± 0.2

GE: grounded electrode (anode); RF: cathode.

[a] RF: RF electrode (cathode), GE: grounded electrode (anode).

[b] RF: power changed during the deposition since the bias voltage was kept constant.

[c] n.d.: not determined.

[d] The E-modulus values of the coatings on the anode are influenced by the substrate. Due to the low thickness and softness of these films, the resulting indentation depth exceeds the maximum indentation depth recommended by the Bückle rule. The values mentioned in the text refer to measurements at a lower load of 10 mN, therefore, the latter values differ from the ones listed in this table.

[e] RF power was kept constant.

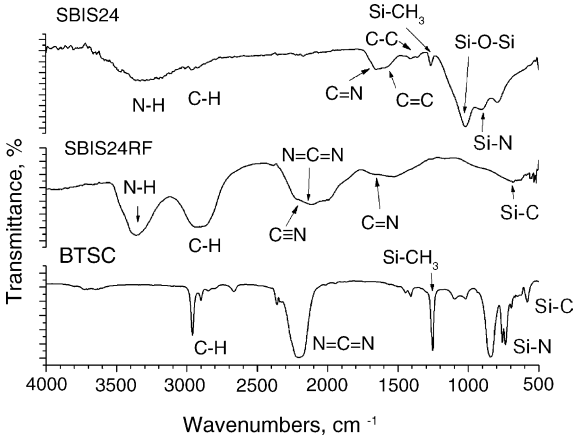

Fig. 2. FTIR spectra of Si/C/N films prepared on metal substrates located at the powered electrode (SBIS24-rf, $T \sim 70\,^{\circ}C$) and the grounded electrode (SBIS24, $T \sim 300\,^{\circ}C$). The IR spectrum of the liquid precursor BTSC is depicted for comparison. The denoted bands are discussed in the text.

they exhibit very different ratios of the elements: Si:C about 1:1 and Si:N about 1:1.7. Therefore, these coatings are rich in nitrogen, while their carbon content is significantly reduced in comparison to films deposited on the grounded electrode. Hydrogen is present in both coatings, approximately to the same amount. For more details of the chemical composition obtained in the GDOES measurements we refer to the data listed in Table 1.

Having established the chemical composition of the coatings we investigated the bonding within the films further using infra-red spectroscopy (FTIR). Fig. 2 shows FTIR spectra of our Si/C/N coatings received at the RF electrode (SBIS24-rf) as well as at the grounded electrode (SBIS24). To allow a comparison with the functional groups of the liquid precursor, a FTIR spectrum of BTSC is included in Fig. 2.

The molecular precursor with its well-defined chemical structure exhibits sharp absorption lines, which have been discussed in more detail elsewhere.[25–27] The bands are typically attributed to localised bonds of the molecule: ν_{as} (C–H) at 2967 cm^{-1} (m), ν_s (C–H) at 2903 cm^{-1} (vw), ν_{as} (N=C=N) at 2205 cm^{-1} (vs), δ_{as} ($SiCH_3$) at 1406 cm^{-1} (vw), δ_s ($SiCH_3$) at 1253 cm^{-1} (s), ρ_{as} (CH_3) at 837 cm^{-1} (vs), ν_{as} (Si–N) at 760 cm^{-1} and ν_{as} (Si–N) or ρ_s (CH_3) at 736 cm^{-1} (s). Similar resonance bands were observed for the silylcarbodiimide units in the crystalline Si/C/N phases silicon dicarbodiimide $Si(NCN)_2$ and silicon carbodiimidenitride $Si_2N_2(NCN)$.[28]

The FTIR spectra of the coatings on the other hand lack sharp absorption lines. The amorphous structure of the films, inherently connected to variations in bond lengths, bond angles, and the local environment of all atoms, is reflected by the rather broad features visible in both spectra. A detailed analysis together with an assignment to distinct structural motives is only possible through careful comparison to the data provided in the literature. Table 2 lists typical wave numbers and corresponding structural units.

The chemical analysis in terms of elemental composition and chemical bonding points to significant and even huge differences between coatings received at the grounded electrode side and at the RF electrode in the CVD chamber. In the following sections we will investigate as to whether these differences are also present in microstructural and mechanical properties of the coatings.

3.2. Morphological characterisation and properties of the coatings

Scanning electron microscopy (SEM) revealed the morphology of the films, as shown in Fig. 3. Here, a cauliflower surface morphology of sample SBIS19-rf is visible. A very similar morphology was found for the other samples as well. Occasionally perfectly circular droplets protrude from the otherwise relatively smooth surface. The majority of these droplets have a diameter of approximately 10 μm (see Fig. 4).

Further surface studies using atomic force microscopy (AFM) revealed the topography of the samples SBIS24-rf and SBIS24, presented in Fig. 5a and b. The figures are also used to determine the surface roughness of both specimens. Within the area of 5 μm × 5 μm we calculate a root mean square value of 4.68 nm and 2.66 nm for SBIS24-rf and SBIS24, respectively. Therefore, some lateral structures larger than 4 nm can be identified on the surface of SBIS24-rf.

The hardness of the amorphous Si/C/N films was measured by indentation tests and the results for a selected sample set are presented in Table 1. The data are averaged plastic hardness values obtained from at least six indentations. The films grown on the cathode side exhibit a hardness from 24 GPa to 30 GPa (see Table 1). On the other hand the films grown on the anode are quite soft. The less ceramised nature of the anode-side films also becomes apparent considering the elastic moduli. While the cathode side coatings exhibit fairly high elastic moduli in the range of 80–110 GPa, the films grown on the anode only have elastic moduli of 21–29 GPa (Determined at 10 mN indentation force. The values given in Table 1 are obtained from measurements at 100 mN. At this force, however, the indentation depth exceeds the 10% rule, resulting in a large substrate influence on the values).

The adhesion of the films was determined by scratch testing. The failure of the coatings is characterised by cohesive and adhesive damages, which are correlated to the normal forces at which they occurred, yielding a critical load (L_c).

In Fig. 6 scratch in a cathode side coating (SBIS20-rf) and the occurring damages are depicted. As the load increases, first cracks appear within the coating (L_{cCrack}) with a curvature mostly in the direction of loading. Then parts of the coating delaminate ($L_{cDelamination}$) from the substrate and chip off. Finally the diamond tip breaks through to the substrate ($L_{cThrough}$). The results for the adhesion testing are presented in Table 3. The critical forces causing a delamination of the film are in the range of 5–10 N.

The wear properties were studied only for hard coatings obtained at the cathode side. In lubricated condition, at a load of 5 N the coating did not show any signs of wear—neither at RT, nor at 100 °C. At 30 N the coating deformed under the

Table 2
Vibrational bands and the corresponding structural features of Si/C/N materials. Typical FTIR spectra obtained in the present study are depicted in Fig. 2

Bond/functional group	Wave number (cm^{-1})	Remarks	References
N—H	∼3350		36
C—H (aliphatic and aromatic)	2850–3050	sp^2- and sp^3-carbon	37,38
C≡N	∼2200		4,9,39,40
C≡N	2264		24
N—CN	2259	ν (C≡N)	27
	1130	ν(C—N)	
N=C=N	2152	$[RSi(NCN)_{1.5}]_n$-gel from BTSC	24,41
N=C=N	2199	ν_{as} (NCN)	27
	1498	ν_s (NCN)	
Si—H	∼2000	Stretching modes	42
C=N	∼2200		43
	∼1600		6,16,16,44
	1650		5
N—C=N	1640	ν_{as} (CN_2)	27
	1322	ν_s (CN_2)	
C=C	1580		6,17
(for $Me_2C{=}CH_2$)	1661	ν (C=C)	27
sp^2-carbon	1550	So-called G-band	45,46
sp^3-carbon	1350	So-called D-band	45,46
$Si(CH_3)_3$	1270	$[RSi(NCN)_{1.5}]_n$-gel from BTSC	24
C—N	1050–1400		47,48
C—N (for Me_2N-X)	880–1100		27
C—N (polymer gel)	∼1578	$[RSi(NCN)_{1.5}]_n$-gel from BTSC	24
C—N	1646		49
C—C	1400 or 1456		6,17,49
Si—O (bulk)	∼1000	Usually very broad	36,38,50,51
SiO_2	1416		27
Me_3Si—O—$SiMe_3$	1059		27
Si—N (bulk)	950	Usually very broad	52,53
Si—N (for Cl_3Si—NHMe)	945		27
Si—N (for Me_3SiNMe_2)	598		27
Si—C (bulk)	780	Usually very broad	39,54
C—Si (for Me_3Si—$SiMe_3$)	720, 688		27
C—Si (for Me_2SiHCN)	560		27
C—Si (for H_3Si—CN)	608		27

Confer the text for a discussion of the data.

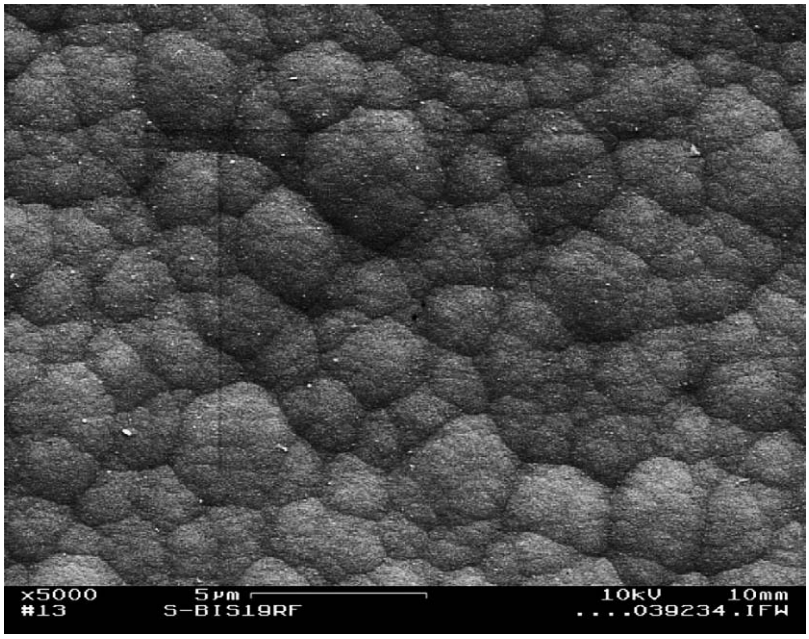

Fig. 3. SEM image of the surface of SBIS19-rf revealing a “cauliflower” morphology.

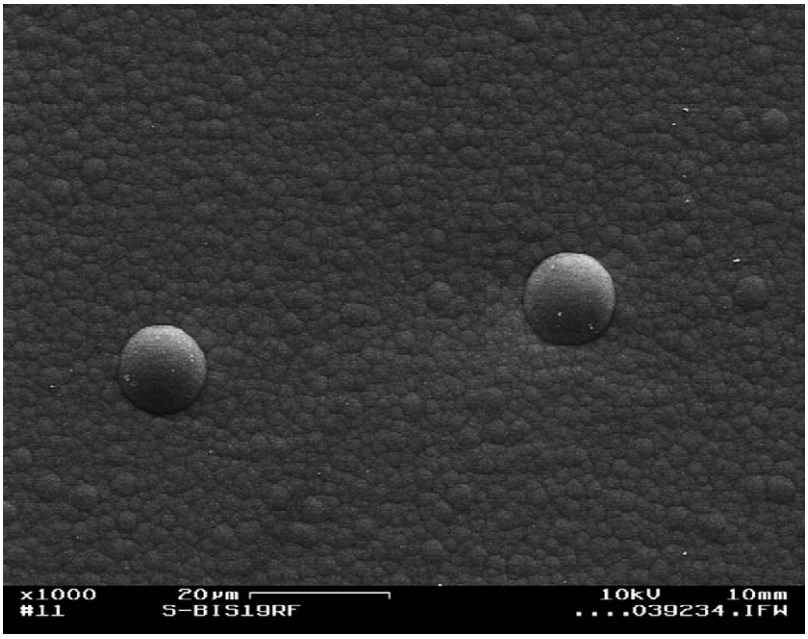

Fig. 4. Surface with droplets of the cathode side film SBIS19-rf.

high Hertzian pressure in the contact zone. The completing of the test cycle resulted in a wear track with a maximum depth of 0.8 μm. However, at 50 N the coating did not withstand the pressure and the test cycle had to be aborted after 5 min (5 min being the minimum testing time for the data recording unit)—the film had chipped off the substrate spaciously around the contact zone.

The tests under dry conditions were conducted with a load of 5 N at RT and at 400 °C. At RT the coating showed strong wear (SBIS19-rf, see Fig. 7). The wear test conducted at 400 °C had to be terminated because of film failure (Fig. 8).

A first look at the corrosion resistance and presence of defects such as pinholes of a coating is possible by subjecting the samples to the salt-spray test according to DIN 50021. The samples withstood this test for 96 h without any sign of corrosion. Measurement of the free corrosion potential showed that the Si/C/N coating is more noble than the S652 HSS substrate material.

The current density–potential curve in 3% NaCl solution (Fig. 9) shows that for the S652 HSS substrate the current density is increasing rapidly when the potential is raised above the free corrosion potential. The material is actively dissolving. The Si/C/N-coated substrate on the other hand remains passive over the whole potential range and protects the substrate from corrosion.

4. Discussion

4.1. Chemical structure of the coatings

Due to the completely amorphous nature of the coatings X-ray and electron diffraction (XRD and SAED using TEM) provide only very limited information of the structure of the coatings on both the anode and the cathode. Therefore, the current discussion of the chemical structure of our films is based on FTIR spectroscopy and the chemical composition as determined by GDOES (and EDX). Future examinations will include XPS and RBS measurements.

The molecular single-source precursor BTSC, which was used for all experiments discussed in this study, has an elemental composition of $Si_2N_2C_7H_{18} = Si_1N_1C_{3,5}H_9$. A comparison with the GDOES data clearly shows that during the fragmentation and deposition process the Si:C as well as the Si:H ratios are decreased significantly in all samples (see Table 1), except for SBIS19. This is due to the formation of alkanes, especially CH_4 and C_2H_6, which are relative stable molecules. Therefore, a large fraction of these species is removed from the deposition sites in the CVD chamber by the carrier gas. Furthermore, the Si:N ratio is decreased in all prepared coatings, with the exception of sample SBIS21. Both observation can be explained by a preferred fragmentation of BTSC to form $Si(CH_3)_3$ cations and $(CH_3)_3Si$-NCN radicals. Obviously, the latter species contributes more to the deposition process, which then explains both the decreased Si:N and Si:C ratios of the coatings if compared to the precursor.

The most striking difference between the coatings obtained at the RF electrode (cathode) and the grounded electrode (anode) is the increased oxygen content of the latter coatings. The high oxygen content might originate from a post deposition ageing of the coatings (i.e., oxidation and hydrolysis) in air.[29] However, the hydrolysis of silyl carbodiimides is known to generate cyanamide H_2N-CN or its derivatives,[23] i.e., C≡N groups, which were not detected

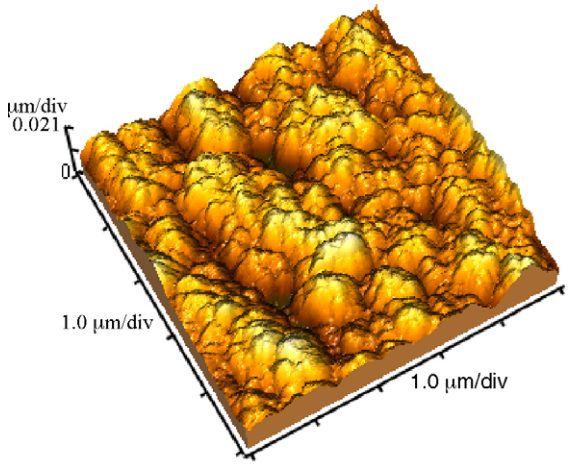

(a) SBIS24-rf, RMS 4.68 nm

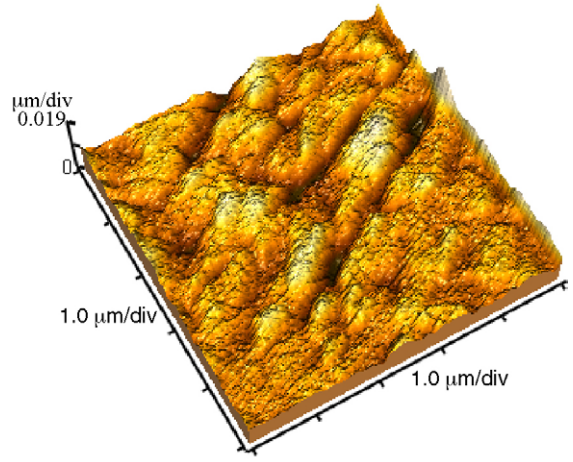

(b) SBIS24, RMS 2.66 nm

Fig. 5. AFM images of the surface topology of the films SBIS24-rf, rms 4.68 nm (a) and SBIS24, rms 2.66 nm (b) (unit: µm/div, for (a) is (5 × 1.0 µm/div) × (5 × 1.0 µm/div) × (2 × 0.021 µm/div), and (b) is (5 × 1.0 µm/div) × (5 × 1.0 µm/div) × (2 × 0.019 µm/div)).

(by FTIR) in these coatings obtained at the grounded electrode.

Another explanation for the very high oxygen content might be the significantly lower deposition rates found for the grounded electrode side. If an equal and constant probability for oxygen incorporation is assumed for a certain oxygen content in the atmosphere of the deposition chamber, the oxygen content of the films should be proportional to $1/r$ (r = deposition rate). This would explain the much higher oxygen content of the films deposited on the grounded electrode (the anode) as compared to the much thicker coatings formed on the cathode.

Table 3
Results from Scratch testing

Probe	L_{cCrack} (N)	$L_{cDelamination}$ (N)	$L_{cThrough}$ (N)
SBiS 20-RF	1	8	11
SbiS P4-RF	2	5	13

Examining the FTIR spectra of the films and comparing them with the spectrum of the molecular precursor as well as with the literature data provides a very different picture of the chemical bonding in coatings obtained at the cathode (the RF side) as well as the anode (see Fig. 2). While both spectra exhibit strong absorption bands at about 3350 cm^{-1} and 3000 cm^{-1}, indicating N–H and C–H bonds, respectively, coatings deposited at the RF electrode show a strong absorption region centred at 2000 cm^{-1}, with a significant broadening and ranging from 2300 cm^{-1} down to 1800 cm^{-1}. It is possible that this band is caused by the presence of N=C=N units, reflecting the dominant functional group of the molecular precursor. It is remarkable that silyl carbodiimide units have been detected in Si/C/N coatings formed by magnetron sputtering, as reported recently.[30] Besides, it is known that Si–NCN–Si groups are stable up to temperatures around 1100 °C.[23] This supports the assignment of the broad band around 2200 cm^{-1} to N=C=N valence modes. Si–H vibrations, however, are also found typically in this region. Hence, a conclusive assignment can not be made. Furthermore, cyanogen units (C≡N) may also contribute to this band. On the contrary, however, a similar band is not visible in films received at the grounded electrode side. There is neither indication for appreciable amounts of Si–H or N=C=N units, nor for C≡N bonds.

Both coatings then show a more or less pronounced absorption band between 1700 cm^{-1} and 1300 cm^{-1}. This can be assigned to C=N and C=C double bonds, but also to delocalised bonds in graphite-type regions, probably with some admixture of nitrogen. These structural features, which might include so-called sp^2-hybridised free carbon, are probably responsible for the black colour of the coatings.[31] A sharp absorption peak at 1270 cm^{-1} is visible only in films deposited on the grounded electrode. This absorption can unambiguously be assigned to residual Si–CH_3 units of the molecular precursor.

A third FTIR characteristic that distinguishes between the two deposition sides in the CVD chamber then is the region below 1200 cm^{-1}, associated with delocalised vibrations of the Si/C/N bulk. The films received on the grounded electrode exhibit the characteristic features associated to Si–O bonds between 1100 cm^{-1} and 1000 cm^{-1}. Coatings deposited at the RF electrode exhibit a less pronounced maximum absorption at around 700 cm^{-1}, which is typical for Si–N and/or Si–C bulk vibrations.

The distinct chemistry as analysed by FTIR of the coating received at cathode and anode is, furthermore, correlated with the mechanical properties (see also Section 4.2). The huge differences in hardness can be attributed to the different local environment of the silicon atoms visible in the spectra: the more Si atoms bonded to C and N, the harder the coating appears; more oxygen in the bulk manifests in a majority of Si–O bonds and results in a deterioration of mechanical properties. The hard coatings obtained at the RF-electrode,

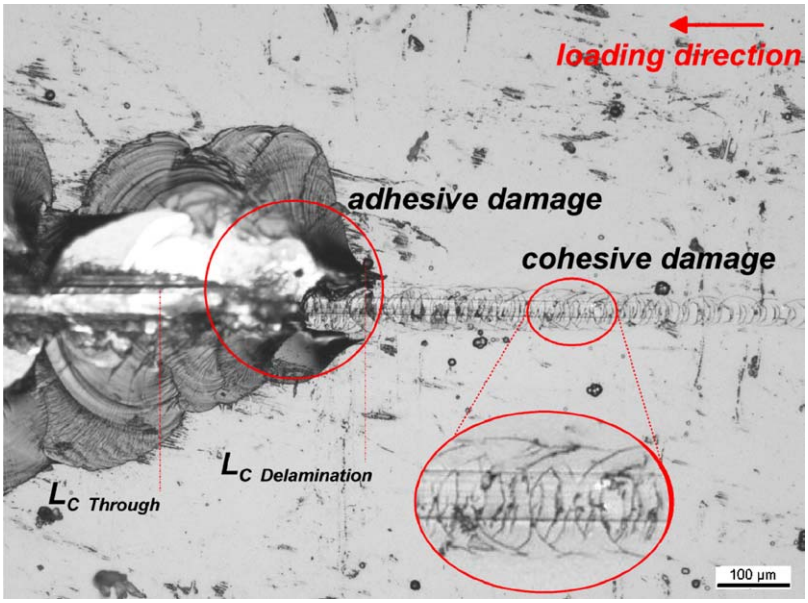

Fig. 6. Optical microscope image of a scratch track showing cohesive and adhesive damages of the coating (SBIS 20-rf). The starting point (L_{cCrack}) of the cohesive damage is to the right outside of the micrograph.

however, still show a significant fraction of residual N–H and C–H bonding. The amount of approximately 20 at.% of hydrogen gives clear reminiscence of the organosilicon single-source precursor used in the CVD. One way of improving mechanical properties and probably the adhesion as well, thus, may be found in reducing the hydrogen content of the coatings.

4.2. Morphology and mechanical properties of the coatings

The properties of any coating material are directly related to its chemical composition and structure on the one hand (see Section 4.1) as well as the morphology on the other hand, which in turn are both controlled by the deposition

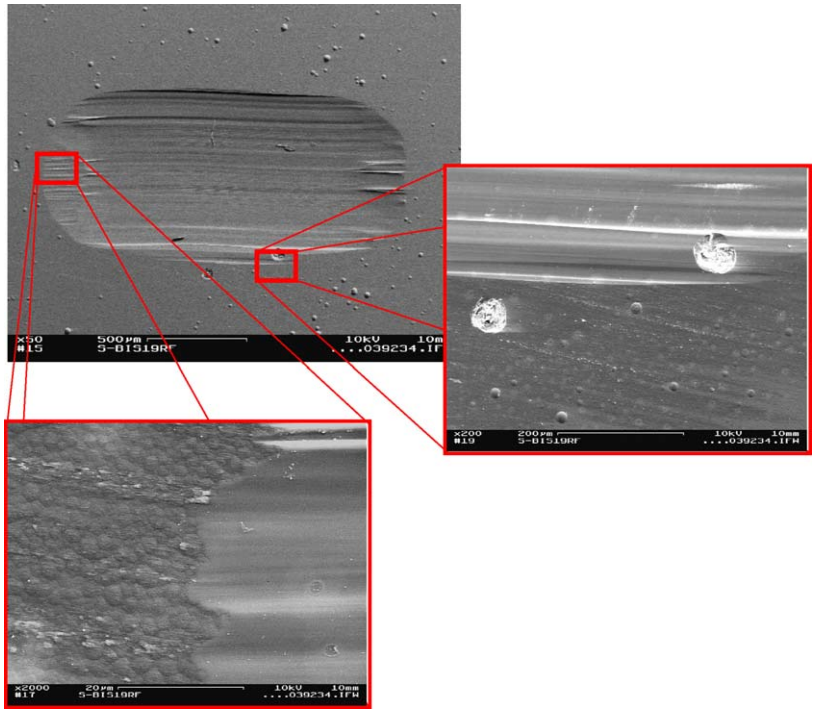

Fig. 7. Wear track at RT: upper frame: wear track at RT; right: chipping off of droplets; lower frame: grooves in the wear zone (SBIS19-rf).

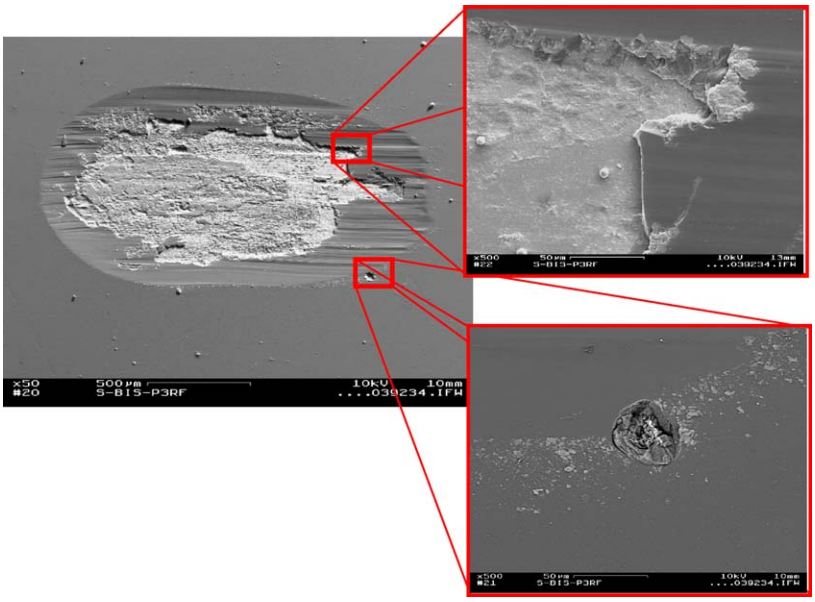

Fig. 8. Wear track on SBIS-P3-rf (RF electrode) coating at 400 °C: left frame: wear track at 400 °C, breakthrough of the substrate, and fretting of the counterbody in the centre of the track; upper right: delamination of the coating; lower right: chipping off of droplets.

conditions. The most desirable coating morphology for load-bearing applications and good mechanical properties, such as high hardness and fracture toughness, consists of a dense (micro)crack-free layer of very fine grains. In general, CVD-synthesised ceramics such as SiO_2 or Si_3N_4 tend to be amorphous or, at least, have a very small grain microstructure.[32] This is also the case for the Si/C/N coatings obtained in our experiments. As already mentioned above, all coatings were completely amorphous according to XRD measurements. Besides, the AFM studies indicate a maximum rms roughness between 2 and 5 nm for an area of 5 μm × 5 μm. Given the film growth with a characterization of cluster stack, therefore, it can be concluded that the primary grain size is in the range, i.e., <5 nm. This corresponds with SEM images of cross-sections of the films, which showed a dense, completely homogenous and featureless morphology.

However, on a larger scale (in the micrometer range) we reproducibly found a cauliflower surface structure as depicted in Figs. 3 and 4. This is usually associated with a low surface mobility during the formation of amorphous coatings at low-temperatures (and high growth rates).[33] Ideally, this structure can be simulated by a random serial deposition of hard balls. However, coatings with cauliflower morphology are often porous. Nevertheless, our samples did not show any signs for open (or closed) porosity. The samples withstood the salt-spray test according to DIN 50021. This clearly indicates the dense and defect free nature of the Si/C/N coatings.

As depicted in Fig. 4, perfectly circular droplets were reproducibly formed. Similar morphologies have been reported[34]: The thermal MOCVD growth of gallium nitride layers from the single-source precursor $[(C_2H_5)_3GaNH_2]_3$ yielded Ga droplets on (or in) the GaN films. This is caused by the relatively low thermal stability of GaN, which decomposes above 700 °C. It is unlikely that a similar mechanism based on decomposition is responsible for the formation of the droplets in the case of the Si/C/N films. Thus, the reasons for the droplet formation remain unclear.

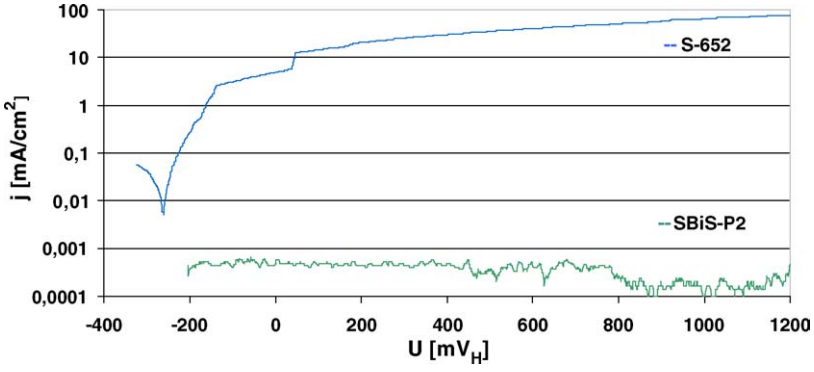

Fig. 9. Comparison of the substrate material S652 high speed steel to the Si/C/N coated substrate in the current density–potential test.

The mechanical properties of the coatings on the RF electrode (cathode) are much more promising than those obtained on the anode. The hardness of the cathode coatings varied between 24 GPa to 30 GPa (see Table 1). This is in the upper range of conventional hard coatings like CrN.[35]

The scratch tests revealed delamination of the film and are in the range of 5 N to 10 N as mentioned above. The early appearance of cracks and spacious delamination suggests that the film is brittle and of low adhesion. Information about the state of the intrinsic stresses in the film can be derived from the shape of the cohesive cracks. The curvature of the cracks predominantly in the direction of loading suggests that the coating is in a state of tensile intrinsic stress. A curvature away from the direction of loading would point to intrinsic compressive stresses.

The wear tests under lubricated condition confirmed the adhesion problem. Due to the brittle nature (qualitatively determined from scratch tests) and the rather poor adhesion of the coating, the film reacts with cracking around the contact zone when its load-bearing capacity is reached. These cracks then lead to broad delamination of the film.

Under dry conditions a tendency to strong groove formation, which is probably caused by abrasion through microchipping of the film material, is evident. Droplets protruding from the surface are braking out of the film and then act as abrasive in the contact zone (right image in Fig. 7).

The premature failure of the film is caused by high tensile intrinsic stresses and the low adhesion of the films on the substrates. The SEM images in Fig. 8 (upper right) show cracks and cleavage within the film around the contact area. Additionally, iron oxide particles were found at the sides of the wear track, which increased the abrasion in the contact area.

For tribological applications, it is important to maintain good adhesion between the substrate and the coating. However, the prepared coatings lack good adhesion to the substrate so far. Therefore, their tribological behaviour was not as good as expected from the high hardness values. Future work will focus on possibilities to enhance the adhesion in order to improve the tribological properties. This can be achieved by modification of the pretreatment and deposition conditions (heating of the substrate, for example) or by the depositing adhesion promoting interlayers before the deposition of the Si/C/N film.

5. Summary and conclusions

Amorphous Si/C/N coatings were deposited on high speed cutting steel S652 substrates by RF-PECVD at low-temperature, using the single-source liquid precursor bis(trimethylsilyl)carbodiimide. The composition and properties of the films strongly depend on the deposition conditions. Hard (22–29 GPa) and thick (>20 μm) Si/C/N films with low oxygen contamination were obtained on the non-heated RF electrode (cathode) with a DC self-bias of 500 V. These coatings contain a relatively large fraction of C–H and N–H units. The surface topology is very smooth with a roughness of 2–4 nm in the area of 5 μm × 5 μm. All coatings produced on the grounded electrode are much thinner (1–3 μm). They contain large amounts of oxygen and are relatively soft. On both electrodes island film growth was observed.

The smoothness, hardness of the Si/C/N films deposited on the RF electrode make them promising candidates for applications in fields such as tribology or cuttings tools. However, in order to improve the tribological properties more research related to adhesion of Si/C/N coatings on the steel substrate is required. Nonetheless, the Si/C/N coatings show an excellent corrosion performance. More testing (especially using different electrolytes) is necessary, however, to fully evaluate the corrosion properties of the coatings.

Acknowledgement

This work was financially supported by the Deutsche Forschungsgemeinschaft (Bonn, Germany) within the framework of DFG-SPP 1119: “Inorganic Materials by Gas Phase Deposition: Interdisciplinary Approaches to Development, Understanding and Control of CVD-Techniques”. We would like to thank Dr. Joachim Brötz and Dr. Helmut Ehrenberg for XRD measurement and analysis, Dr. Dirk Hegemann for useful discussions on PECVD in general, and Prof. Dr. Heinz von Seggern and Mr. Marcus Ahles for access to the ellipsometer.

References

1. Riedel, R., Kleebe, H. J., Schoenfelder, H. and Aldinger, F., *Nature*, 1995, **374**, 526.
2. Badzian, A., Badzian, T., Drawl, W. D. and Roy, R., *Diam. Relat. Mater.*, 1998, **7**, 1519.
3. Zhang, W., Zhang, K. and Wang, B., *Mater. Sci. Eng.*, 1994, **B26**, 133.
4. Xiao, X., Li, Y., Song, L., Peng, X. and Hu, X., *Appl. Surf. Sci.*, 2000, **156**, 155.
5. Peng, X., Song, L., Meng, J., Zhang, Y. and Hu, X., *Appl. Surf. Sci.*, 2001, **173**, 313.
6. Sundaram, K. B. and Alizadeh, J., *Thin Solid Films*, 2000, **370**, 151.
7. Machorro, R., Samano, E. C., Soto, G. and Cata, L., *Appl. Surf. Sci.*, 1998, **127–129**, 564.
8. Kleps, I., Angelescu, A., Caccavale, F., Brusatin, G. and Armelao, L., *Vacuum*, 1995, **46**, 979.
9. Chen, L.-Y. and Hong, F. C.-N., *Diamond Relat. Mater.*, 2003, **12**, 968–973.
10. Fainer, N. I., Rumyantsev, Yu. M., Golubenko, A. N., Kosinova, M. L. and Kuznetsov, F. A., *J. Cryst. Growth*, 2003, **248**, 175–179.
11. Marx, G., Koerner, K.-U. and Heger, P., *Steel Res.*, 2001, **72**, 518–521.
12. Wilden, J., Wank, A., Asmann, M., Heberlein, J. V. R., Boulos, M. I. and Gitzhofer, F., *Appl. Organomet. Chem.*, 2001, **15**, 841–857.
13. Kuo, D.-H. and Yang, D.-G., *Thin Solid Films*, 2000, **374**, 92–97.
14. (a) Bendeddouche, A., Berjoan, A., Beche, E., Merle-Mejean, T., Schamm, S., Serin, V. *et al.*, *J. Appl. Phys*, 1997, **81**, 6147;
(b) Bendeddouche, A., Berjoan, A., Beche, E. and Hillel, R., *Surf. Coat. Technol.*, 1999, **111**, 184–190.

15. Kamata, K., Maeda, Y. and Moriyama, M., *J. Mater. Sci. Lett.*, 1986, **5**, 1051.
16. Zhang, W. and Wang, J. T., *Surf. Coat. Technol.*, 1991, **50**, 11.
17. Chen, L. C., Chen, K. H., Wei, S. L., Kichambare, P. D., Wu, J. J., Lu, T. R. *et al.*, *Thin Solid Films*, 1999, **355/356**, 112.
18. Chen, K. H., Wu, J. J., Chen, C. Y., Chen, L. C., Fan, C. W., Kuo, P. F. *et al.*, *Thin Solid Films*, 1999, **355/356**, 205.
19. Riedel, R., Seher, M., Mayer, J. and Szabo, D. V., *J. Eur. Ceram. Soc.*, 1995, **15**, 703.
20. Dressler, W. and Riedel, R., *Int. J. Refract. Met. Hard Mater.*, 1997, **15**, 13.
21. Kroke, E., Li, Y. L., Konetschny, C., Lecomte, E., Fasel, C. and Riedel, R., *Mater. Sci. Eng. R*, 2000, **26**, 97.
22. Berger, C., Broszeit, E., Falk, F., Hoche, H., Kroke, E., Kroll, P. *et al.*, *Chemical Vapor Deposition XVI and EUROCVD 14, Vol 1* (ISBN 1-56677-380-6). The Electrochemical Society Inc., Pennigton, NJ, USA. *Proceedings, Vol 2003-08*, pp. 646–652.
23. (a) Riedel, R., Kroke, E., Greiner, A., Gabriel, A. O., Ruwisch, L., Nicolich, J. *et al.*, *Chem. Mater.*, 1998, **10**, 2964–2979;
    (b) Kim, D. S., Kroke, E., Riedel, R., Gabriel, A. O. and Shim, S. C., *J. Appl. Organomet. Chem.*, 1999, **13**, 495–499;
    (c) Iwamoto, Y., Völger, W., Kroke, E., Riedel, R., Saitou, T. and Matsunaga, K., *J. Am. Ceram. Soc.*, 2001, **84**, 2170–2178.
24. Gabriel, A. O., Riedel, R., Storck, S. and Maier, W. F., *Appl. Organomet. Chem.*, 1997, **11**, 833.
25. Drake, J. E., Hemmings, R. T. and Henderson, E., *J. Chem. Soc. Dalton Trans.*, 1976, 366.
26. Obermeyer, A., Kienzle, A., Weidlein, J., Riedel, R. and Simon, A., *Z. Anorg. Allg. Chem.*, 1994, **620**, 1357.
27. Weidlein, J., Mueller, U. and Dehnicke, K., *Schwingungsfrequenzen*. Georg Thieme Verlag Stuttgart, New York, 1986.
28. (a) Greiner, A., Dissertation, TU Darmstadt, 1998;
    (b) Riedel, R., Greiner, A., Miehe, G., Dressler, W., Fuess, H., Bill, J. *et al.*, *Angew. Chem. Int. Ed. Engl.*, 1997, **36**, 603;
    (c) *Angew. Chem.*, 1997, **106**, 657.
29. Fracassi, F. and Lamendola, R., *Plasma Polymers*, 1997, **2**, 25.
30. Lutz, H., Dissertation, University of Karlsruhe, 2001 [in German].
31. Trassl, S., Motz, G., Roessler, E. and Ziegler, G., *J. Non-Cryst. Solids*, 2001, **293-295**, 261.
32. Pierson, H. O., *Handbook of Chemical Vapor Deposition (CVD)—Principles, Technology and Applications* (*2nd ed.*). Noyes Publications, Norwich, USA, 1999, Chapter 4.5.
33. Hitchman, M. L. and Jensen, K. F., ed., *Chemical Vapor Deposition—Principles and Applications*. Academic Press, London, 1993 [chapters 2.3, 7 and 10.2.2].
34. Park, H.-S., Waezsada, S. D., Cowley, A. H. and Roesky, H. W., *Chem. Mater.*, 1998, **10**, 2251.
35. Hoche, H., Scheerer, H., Fritsche, R., Thießen, A., Flege, S., Broszeit, E. *et al.*, *Mat.-wiss. U. Werkstofftech.*, 2002, **33**, 132–141.
36. Socrates, G., *Infrared Characteristic Group Frequencies*. Wiley, Chichester, 1994.
37. Andujar, J. L., Viera, G., Polo, M. C., Maniette, Y. and Bertran, E., *Vacuum*, 1999, **52**, 153.
38. Theil, J. A., Brace, J. G. and Knoll, R. W., *J. Vac. Sci. Technol.*, 1994, **A12**, 1365.
39. Gomez, F. J., Martinez, J., Garrido, J., Gomez-Aliexandre, C. and Piqueras, J., *J. Non-Cryst. Solids*, 1995, **191**, 164.
40. Zhang, Z. J., Fan, S. and Lieber, C. M., *Appl. Phys. Lett.*, 1995, **66**, 3582.
41. Wu, J. J., Wu, C.-T., Liao, Y.-C., Lu, T.-R., Chen, L. C., Chen, K. H. *et al.*, *Thin Solid Films*, 1999, **355/356**, 417.
42. Park, J-H., Kwon, H.-S. and Lee, J-Y., *J. Appl. Phys.*, 1992, **72**, 5246.
43. Chen, M. Y., Lin, X., Dravid, V. P., Chung, Y. W., Wong, M. S. and Sproul, W. D., *Surf. Coat. Technol.*, 1992, **54**, 360.
44. Ricci, M., Trinquecoste, M., Auguste, F., Canet, R., Delhaes, P., Guimon, C. *et al.*, *J. Mater. Res.*, 1993, **8**, 480.
45. Nemanich, R. J. and Solin, S. A., *Phys. Rev. B*, 1979, **B20**, 392.
46. Tuinstra, F. and Koenig, J. L., *J. Chem. Phys.*, 1970, **53**, 1126.
47. Li, D., Cutiongco, E., Chung, Y. W., Wong, M. S. and Sproul, W. D., *Surf. Coat. Technol.*, 1994, **68**, 611.
48. Bousetta, A., Lu, M., Bensaoula, A. and Schultz, A., *Appl. Phys. Lett.*, 1994, **65**, 696.
49. Badzian, A., Badzian, T., Roy, R. and Drawl, W. D., *Thin Solid Films*, 1999, **354**, 148.
50. Zhang, J., Wavhal, D. S. and Fisher, E. R., *J. Vac. Sci. Technol. A*, 2004, **22**, 201.
51. Vanhulsel, A., Dekempeneer, E., Smeets, J. and Celis, J. P., *J. Vac. Sci. Technol.*, 1999, **A17**, 2378.
52. Adams, A. C., *Solid State Technol.*, 1983, **23**, 135.
53. Wada, N., Solin, S. A., Wong, J. and Prochazka, S., *J. Non-Cryst. Solids*, 1981, **43**, 7.
54. Chayahara, A., Masuda, A., Imura, T. and Osaka, Y., *Jpn. J. Appl. Phys.*, 1986, **25**, L564.